

## Supplementary Material

### Preparation of tough, high modulus and creep resistant PS/SIS/Halloysite blend nanocomposites

Emre Tekay

Department of Polymer Engineering, Yalova University, Yalova, 77200, Turkey

E-mail: [emre.tekay@yalova.edu.tr](mailto:emre.tekay@yalova.edu.tr)

#### SEM Analysis of HNT Clay

The average primary particle size of the HNT aggregates was found to be 6.1  $\mu\text{m}$ , and used as received (Figure S1).

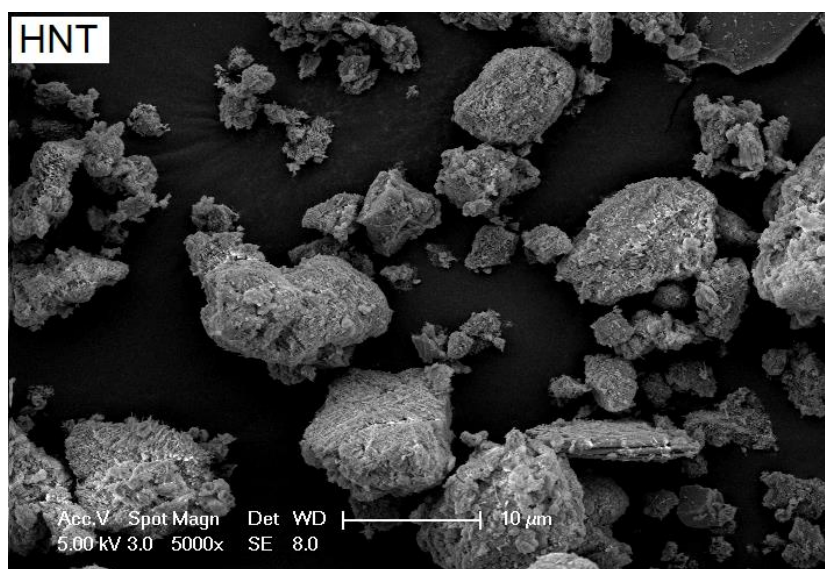
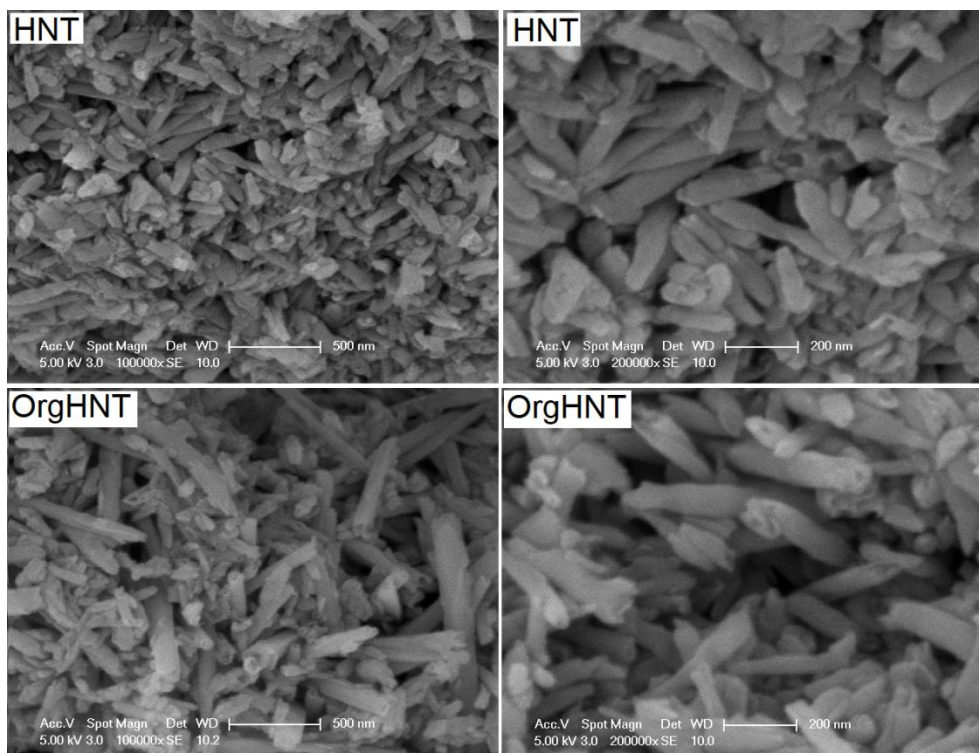


**Figure S1.** Low-magnification SEM images of HNT clay.

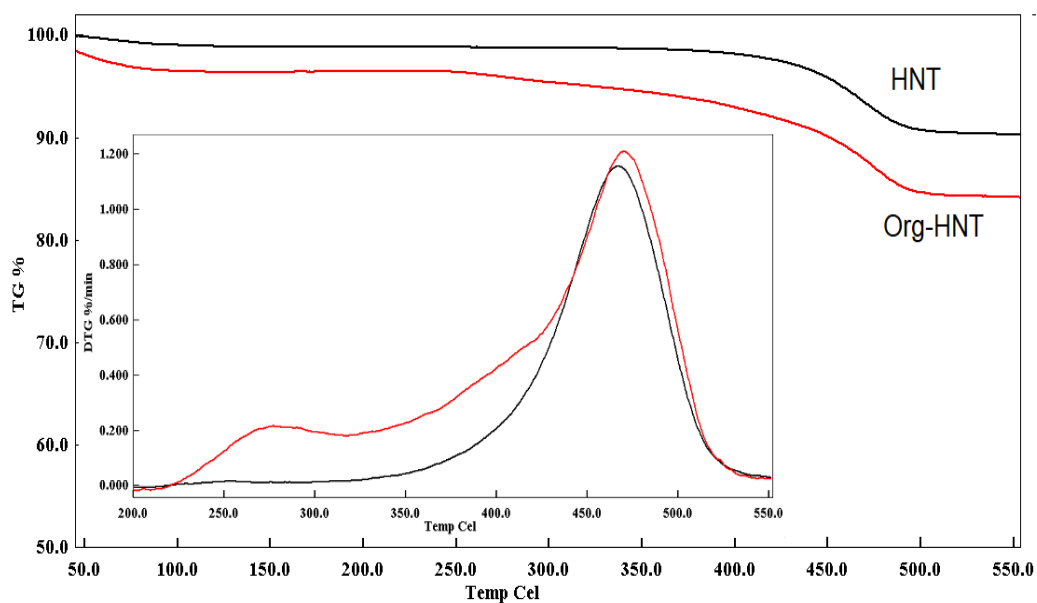
### **Clay Modification**

Figure S2 shows low- and high magnification SEM images of neat HNT and Org-HNT clays. As it is clear from the SEM images, the neat HNTs are in form of aggregates due to their intertubular interactions.<sup>1</sup> The Org-HNT's SEM image, on the other hand, exhibits the nanotubes which are separated from each other after the organophilic modification probably due to loosened intertubular interactions. It can be also noticed from the high-magnification SEM image of Org-HNT that some of nanotube ends are deformed and enlarged which may be resulted from diffusion of the dimethyl-dehydrogenated tallow quaternary ammonium chloride having to long alkyl chains through alumina silicate layers and HNT lumens. This distortion and the separation of the nanotubes providing with an increased surface area can also be due to ion exchange of the quaternary ammonium salt with  $\text{SiO}^-$  groups at the tube ends,<sup>1</sup> which can be expected to lead to a better nanotube dispersion in polymer matrix and elastomer phase as well as much higher interactions with them.

Figure S3 shows TGA thermograms of HNT clays and their derivative curves. The weight loses of the both clay in the temperature range of 420-500 °C results from removal of crystal water present in the nanotube structure.<sup>1</sup> On the other hand, the Org-HNT clay was found to have a higher degradation dependent weight loss in the temperature range of 240-420 °C due to decomposition of quaternary ammonium salt bound to the nanotube surface. The amount of weight loss in that range is almost 4.4 % as the amount of the ammonium salt attached.



**Figure S2.** SEM images of HNT and Org-HNT at different magnifications



**Figure S3.** TGA thermograms and DTG curves of HNT and Org-HNT clays

FTIR spectra of HNT and Org-HNT are given in Figure S4. The peaks at  $3695$  and  $3622\text{ cm}^{-1}$  of the HNT clay are due to O-H stretching of its inner hydroxyl groups. The O-H deformation of the water appeared at  $1635\text{ cm}^{-1}$ .<sup>2, 3</sup> The peaks at  $1120\text{ cm}^{-1}$  and,  $911\text{ cm}^{-1}$  and  $1008$

$\text{cm}^{-1}$  and are assigned to Si–O stretching (outer siloxane groups) bands and, Al–OH (inner/edge hydroxyl groups) bending vibrations and, respectively.<sup>2–4</sup> The shifts of these peaks observed in the spectrum of Org-HNT can be ascribed to ion-dipole interactions between the quaternary ammonium salt and Si–O and Al–OH groups of HNT clay. Moreover, the peaks appeared at 2853  $\text{cm}^{-1}$  and 2925  $\text{cm}^{-1}$ , and 1467  $\text{cm}^{-1}$  in the spectrum of Org-HNT correspond to C–H stretching vibrations and C–H scissoring, respectively owing to the organic group of the Org-HNT clay.<sup>2</sup>

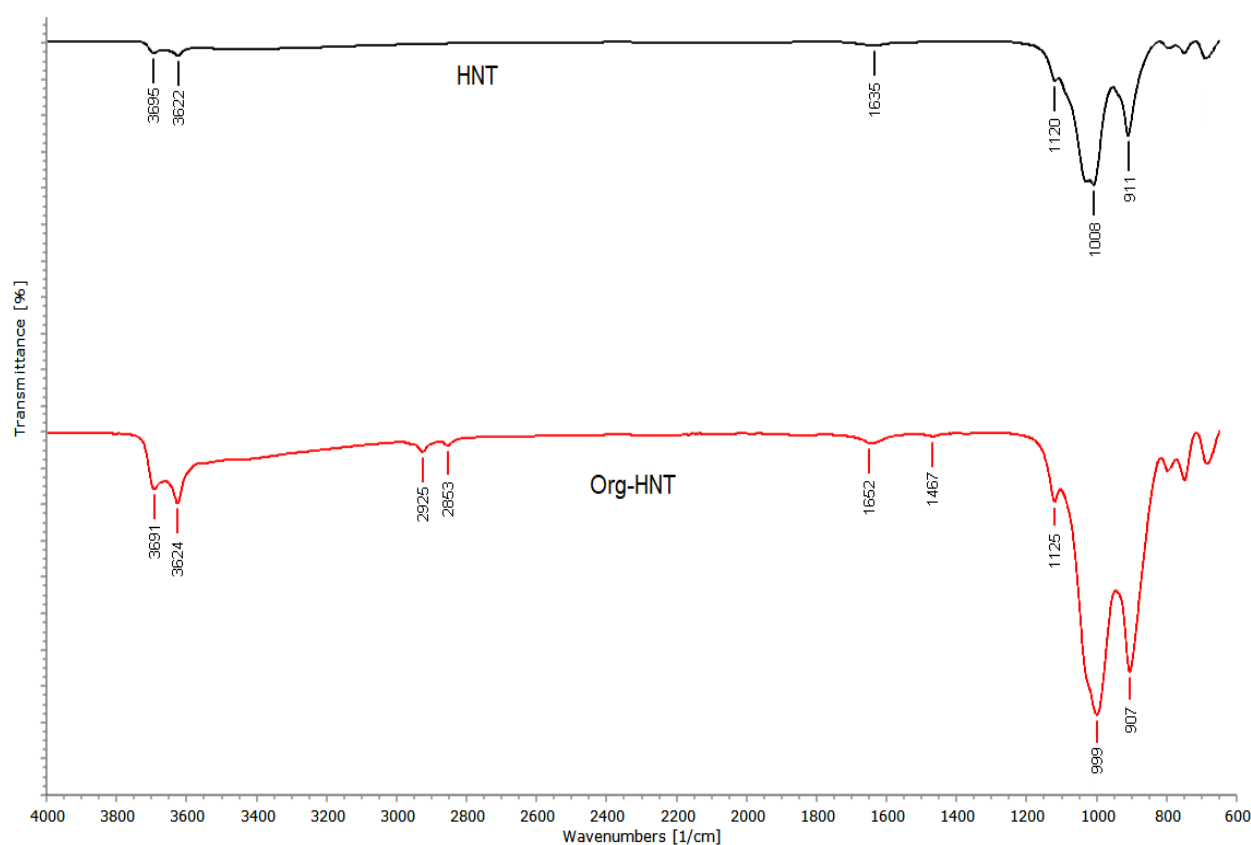


**Figure S4.** FTIR spectra of HNT and Org-HNT clays

XRD curves of the nanotubes are shown in Figure S5. The three characteristic reflections of neat HNT was observed at  $2\theta$  of  $11.98^\circ$ ,  $20.00^\circ$  and  $24.56^\circ$ .<sup>5</sup> The existence of these peaks in XRD data after the organophilic modification is an indication of preservation of the tubular geometry for the clay.<sup>6</sup> The XRD peak representing  $d_{001}$  basal plane of the nanotube was

found to be at  $2\theta$  of  $11.98^\circ$  with a d-spacing of  $7.38 \text{ \AA}$ . This peak shifted to a lower diffraction angle ( $2\theta = 11.90^\circ$ ) with an increase in the d-spacing ( $7.43 \text{ \AA}$ ) for Og-HNT clay. This slight increase in the spacing can be ascribed to the intercalation of some quaternary ammonium salt molecules between alumina silicate layers of the nanotube.<sup>7</sup>

All the SEM, TGA FTIR and XRD data indicate that the dimethyl-dehydrogenated tallow quaternary ammonium chloride as the modification agent interacted with the clay surface and organophilic modification was done successfully.

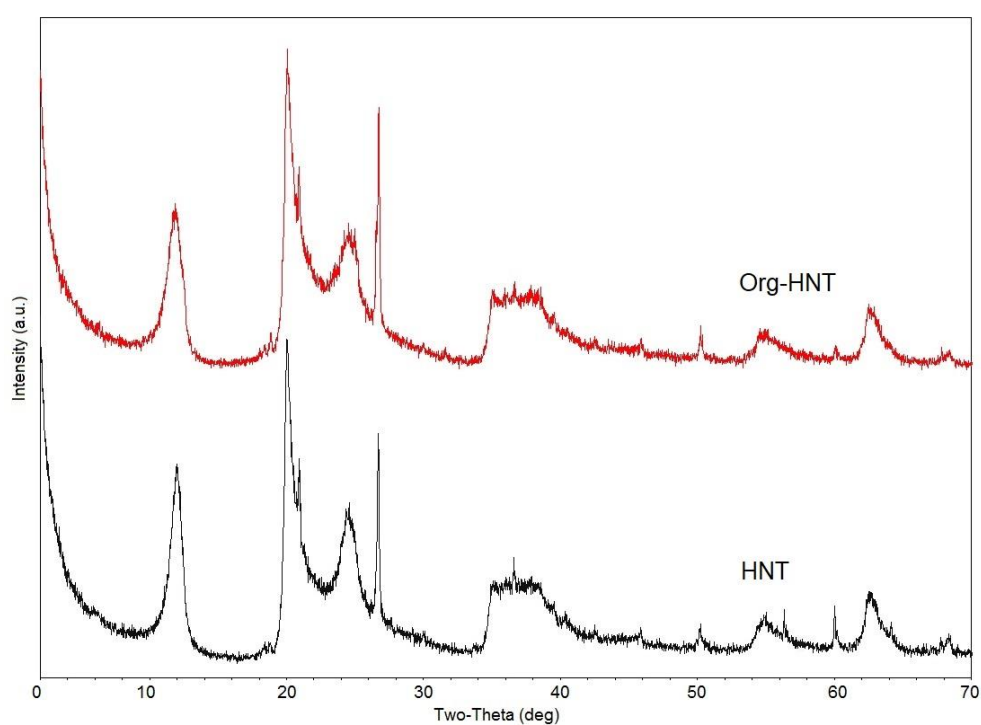


**Figure S5.** XRD curves of the nanotubes



### SEM Analyses of PS-30SIS blend and its composites

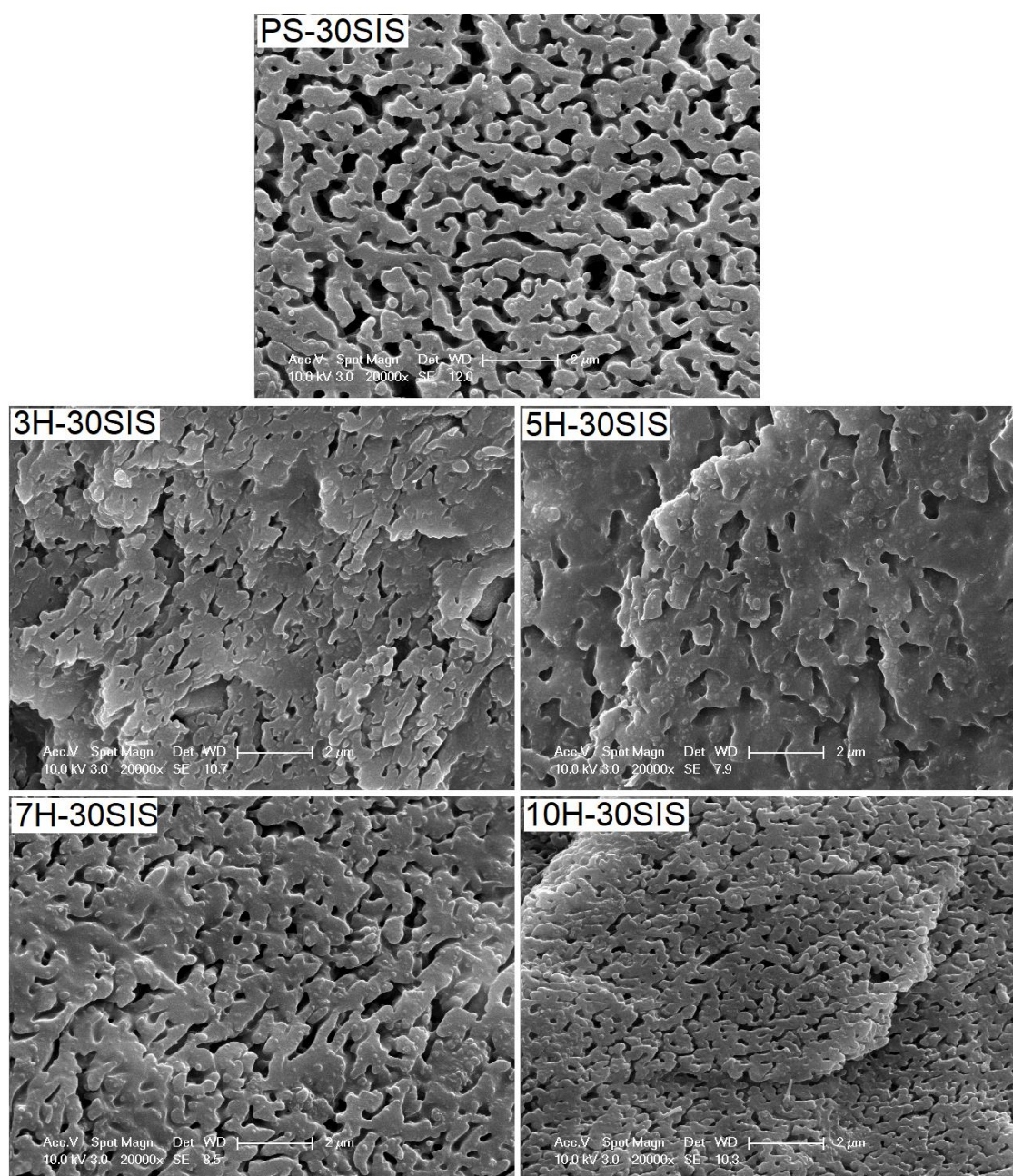


**Figure S6.** SEM images of fractured and etched surfaces of PS-30SIS blend and its nanocomposites (Mag: x 20 000)

**TEM Analyses of PS-30SIS blend nanocomposites**

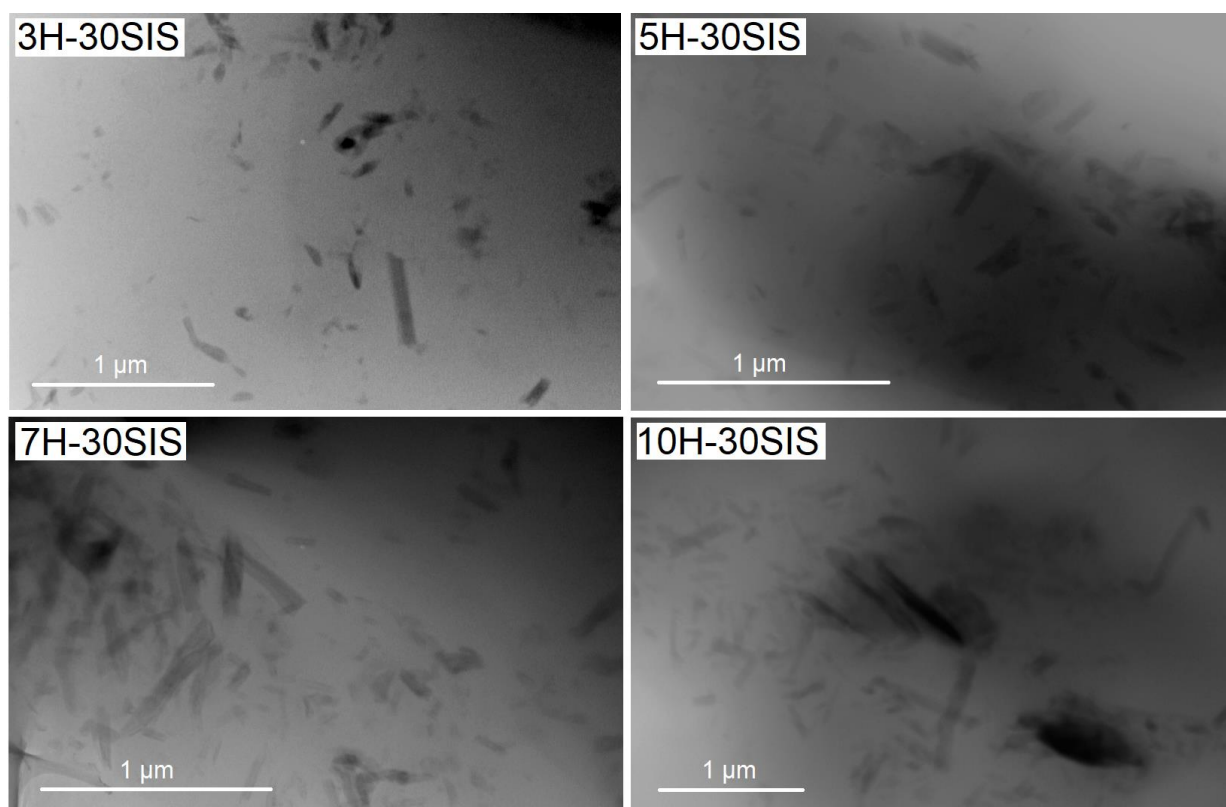


**Figure S7.** TEM images of PS-30SIS blend nanocomposites

### DSC Analyses of PS, PS-30SIS blend and blend nanocomposites

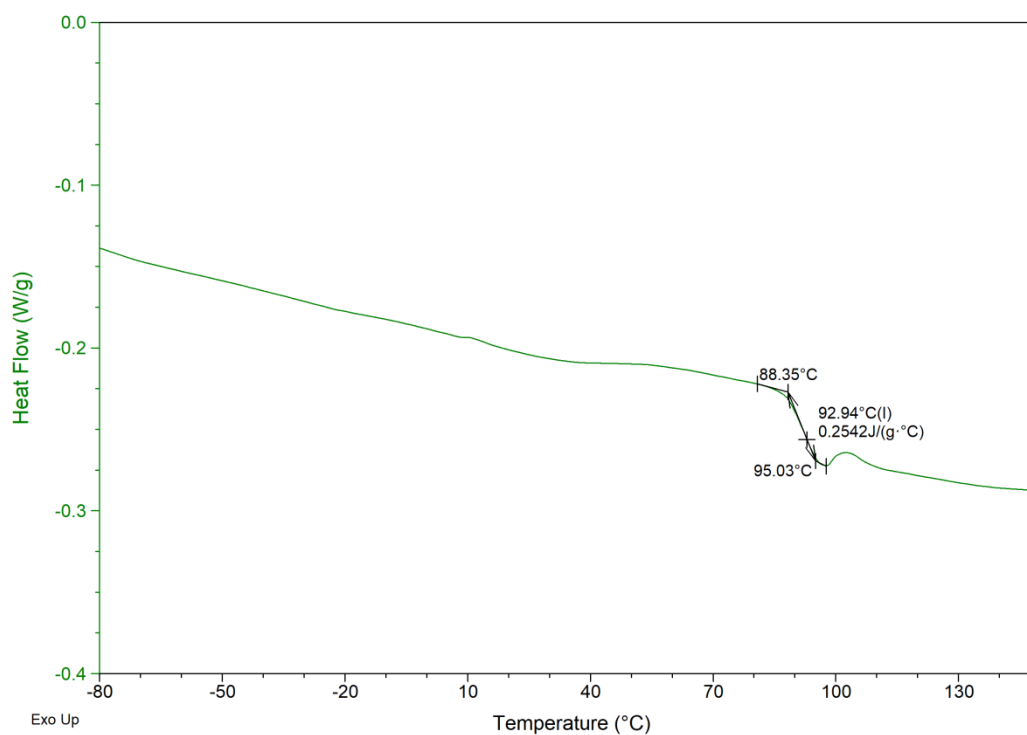


**Figure S8.** DSC thermogram of PS showing its T<sub>g</sub> and ΔC<sub>p</sub> value

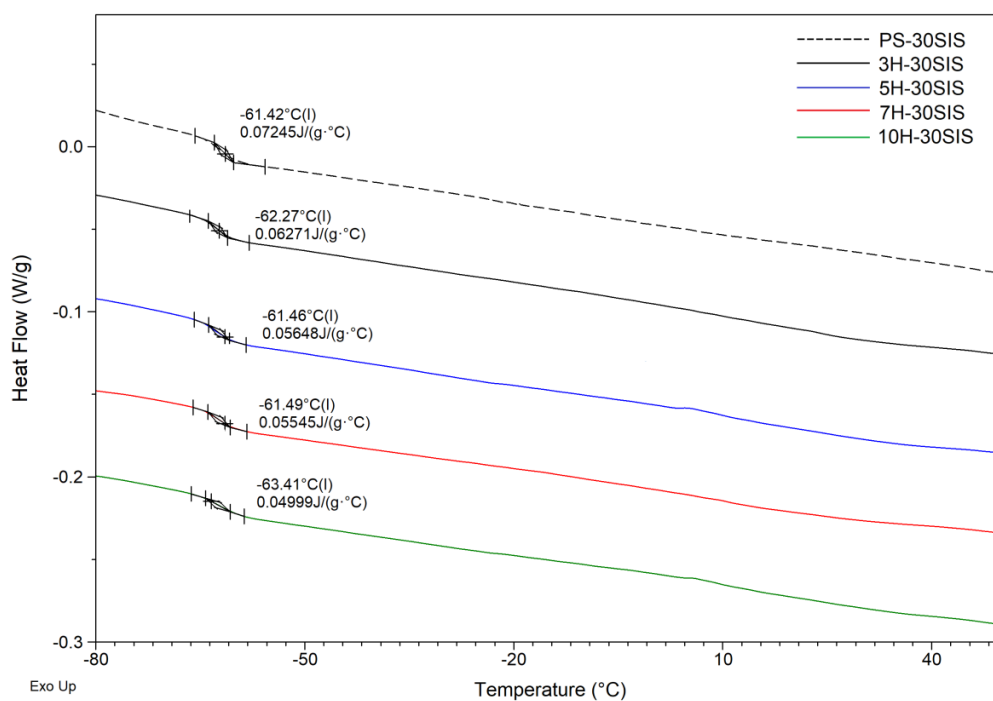


**Figure S9.** DSC thermograms of PS-30SIS and its nanocomposites showing T<sub>g</sub> and ΔC<sub>p</sub> values of polyisoprene



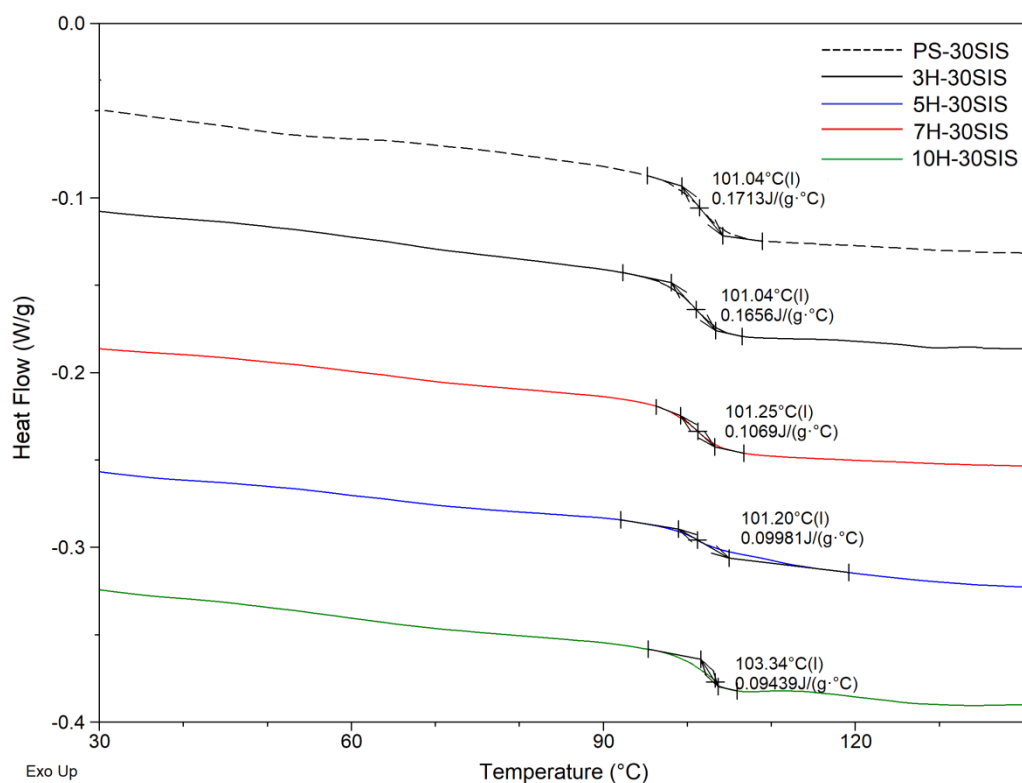


**Figure S10.** DSC thermograms of PS-30SIS and its nanocomposites showing T<sub>g</sub> and ΔC<sub>p</sub> values of polystyrene

## References

1. Tekay E, Nugay N, Nugay T, et al. Revolution/rotation-type mixing-assisted masterbatch process for polypropylene-based high-impact ternary nanocomposites. *Polym Compos* 2019; 40: 24-36.
2. Tekay E, Nugay N, Nugay T, et al. Tuning of nanotube/elastomer ratio for high damping/tough and creep resistant polypropylene/SEBS-g-MA/HNT blend nanocomposites. *J Compos Mater* 2019; 53: 1005-1022.
3. Jamaludin NA, Inuwa IM, Hassan A, et al. Mechanical and thermal properties of SEBS-g-MA compatibilized halloysite nanotubes reinforced polyethylene terephthalate/polycarbonate/nanocomposites. *J Appl Polym Sci* 2015; 132.
4. Zhou X, Zhang Q, Wang R, et al. Preparation and performance of bio-based carboxylic elastomer/halloysite nanotubes nanocomposites with strong interfacial interaction. *Composites Part A* 2017; 102: 253-262.
5. He Y, Xu W, Tang R, et al. pH-Responsive nanovalves based on encapsulated halloysite for the controlled release of a corrosion inhibitor in epoxy coating. *RSC Advances* 2015; 5: 90609-90620.
6. Weibo H and Fengchang Z. Studies on the dynamic mechanical and vibration damping properties of polyether urethane and epoxy composites. *J Appl Polym Sci* 1993; 50: 277-283.
7. Arman N, Tekay E and Şen S. Preparation of high-strength SEBS nanocomposites reinforced with halloysite nanotube: Effect of SEBS-g-MA compatibilizer. *J Thermoplast Compos Mater* 2019; <https://doi.org/10.1177/0892705719895055>.